0.1. Texture representation

Texture refers to the existence of different spatial orientation of the crystalline lattice in different constituents of a polycrystalline assembly. Electron microscopy techniques, such as electron back-scatter diffraction (EBSD), are typically used to measure lattice orientations and obtain orientation distribution functions (ODF). EBSD with high spatial resolution can provide ODF of nanometre-scale microstructures [1]. ODF control the macroscopic material properties, but its evolution during CDRX remains a controversial subject [2].

Generally, ODF can be incorporated in a polycrystalline assembly by assigning crystallographic orientations to all grains (cells of the corresponding polyhedral assembly). A typical EDSD measurement provides the orientation of the crystalline lattice at each spatial position with respect to a fixed external coordinate system in terms of Euler angles (ϕ_1, ϕ, ϕ_2). These can be converted to unit quaternions, $g = (g_0, g_1, g_2, g_3)$, which are more computationally efficient and avoid the singularity at $\phi = \pi/2$ [3, 4]. The vector part (g_1, g_2, g_3) is a rotation axis - a vector with respect to the external coordinate system. The scalar part is $g_0 = cos(\theta/2)$, where θ is the angle of rotation, by which the local lattice triad needs to be rotated around the axis to coincide with the external coordinate system.

The misorientation between two adjacent grains is the rotation required to transform a tensorial quantity, such as stress or strain, from one set of crystal axes to the other [5, 6]. The misorientation that transforms quantities from grain A to grain B can be calculated by $\Delta g_{AB} = g_B \circ g_A^{-1}$, where g_A^{-1} is the inverse quaternion. This is illustrated in Fig. 1. Generally, the rotation angle of the quaternion Δg_{AB} is in the interval $[0, \pi]$. However, the presence of crystal symmetry reduces the possible rotation angles. For example, FCC crystals have 24 symmetrically related orientations, which are physically indistinguishable, but mathematically distinct. The crystal symmetries are represented by crystal symmetry operators S, so that the true misorientation quaternion, referred to as the disorientation, is obtained by [7]:

$$\Delta g_{AB} = S_B \circ g_B \circ (S_A \circ g_A)^{-1}. \tag{1}$$

A map of orientations to all grains/cells provide complete system information, from which the disorientation distribution at grain boundaries/faces can be calculated by Eq. 1. An example of disorientation angle distribution is shown in Fig. 2. The calculated disorientation quaternions between adjacent grains can be assigned to their common boundary in the polycrystalline assembly (the common face in the corresponding polyhedral assembly).

However, the information provided by disorientation quaternions is too complex for characterising the evolution of grain boundaries during CDRX, in particular for calculating global parameters, such as entropy and energy. It is practical to consider a simplified model with a discrete set of grain boundary types. Some past works classify the boundaries into discrete sets on the base of the coincident cite lattice model [8, 9, 10], which is one effective classification of GB networks. For the purposes of the present work, however, a simpler binary

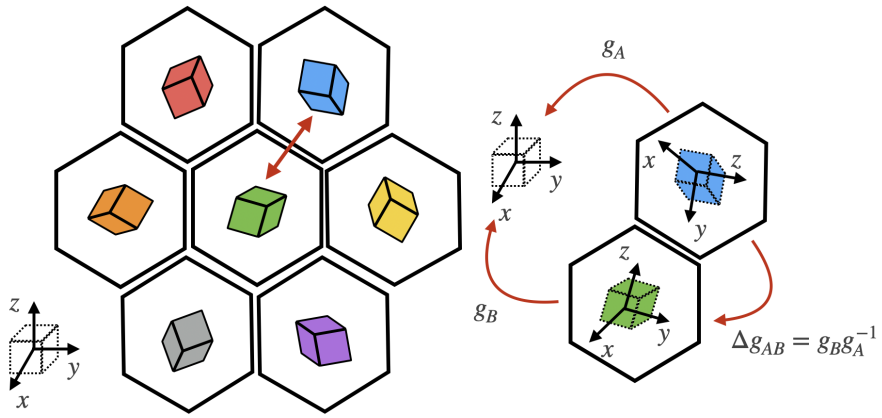

Figure 1: Orientations of crystallographic axes in different structural element with respect to an external reference frame; Misorientation describing transformation between crystal reference frames across a boundary element.

classification is more appropriate [11, 12, 13]. This separates the grain boundaries according to the disorientation angle: low-angle grain boundaries (LAGBs) are those with disorientation angle less than 15 degrees; high-angle grain boundaries (HAGBs) are those with disorientation angle greater greated than 15 degrees. Considering the binary classification of GBs, the TJs are classified into four sets as shown in Fig. 3; J_i is a triple junction that is on the boundary of i HAGBs, $i \in [0, 1, 2, 3]$.

0.2. Discrete cell complexes

An assembly of polyhedrons, denoted by $\mathcal{M}$, is a geometric realisation of a combinatorial structure referred to as cell complex in algebraic topology [14]. From a topological perspective, a microstructure is a 3-complex – a collection of cells with different topological dimensions. A p-cell in $\mathcal{M}$ represents a vertex, an edge, a polygonal face, and a polyhedron for $p = 0, 1, 2, 3$, respectively. These are illustrated in Fig. 4. Such a description is also used in molecular dynamics [15], phase-field method [16], and other simulation approaches [17, 18].

Let σ_p denote an arbitrary p-cell and N_p be the number of p-cells in $\mathcal{M}$. The relation $\sigma_p \prec \sigma_{p+1}$ will mean that σ_p is incident on (on the boundary of) σ_{p+1}. A formal linear combination of p-cells is called a p-chain and denoted by c_p. The p-chains in $\mathcal{M}$ form a vector space, denoted by C_p, with individual p-cells as basis. The cells of the complex are assigned orientations. A standard way is to decide on a consistent orientation of all top-dimensional cells, e.g., to select the positive orientation to be from interior to exterior of the 3-cells and assign arbitrary orientations for all lower-dimensional cells [19]. There are exactly three options for the relation between σ_p and σ_{p+1} in an oriented complex: $\sigma_p \not\prec \sigma_{p+1}$, encoded by 0; $\sigma_p \prec \sigma_{p+1}$ and they have consistent orientations, encoded by 1;

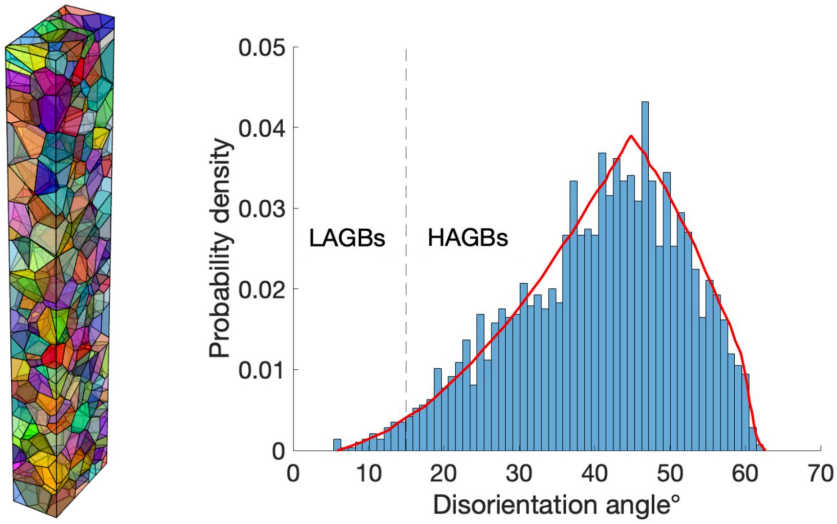

Figure 2: (a) Polycrystalline assembly of 500 grains with randomly assigned lattice orientations; (b) Calculated disorientation angle distribution (bar chart) and distribution for random texture from Mackenzie(1958) (curve).

$\sigma_p \prec \sigma_{p+1}$ and they have opposite orientations, encoded by -1. These relations are collected in a set of boundary operators, ∂_p for $p = 1, 2, 3$, which describe simultaneously the topological structure of $\mathcal{M}$ and operations on chains: ∂_p maps p-chains to $(p-1)$-chains, $\partial_p : C_p \to C_{p-1}$, with the property $\partial_{p-1} \circ \partial_p = 0$, i.e., the boundary of a boundary is empty. Algebraically, ∂_p is a matrix of dimensions $N_{p-1} \times N_p$. Furthermore, $\partial_0 = 0$, i.e., the boundaries of 0-cells are empty, and $\partial_4 = 0$, i.e., the 3-cells are not boundaries of higher-dimensional cells.

The boundary operators are used to form combinatorial Laplacians that map p-chains to p-chains, $L_p : C_p \to C_p$, for $p = 0, 1, 2, 3$. Algebraically, these are matrices of dimensions $N_p \times N_p$ obtained by

$$L_p = \partial_p^T \circ \partial_p + \partial_{p+1} \circ \partial_{p+1}^T. \tag{2}$$

Notably, $L_0 = \partial_1 \circ \partial_1^T$, and $L_3 = \partial_3^T \circ \partial_3$. Combinatorial Laplacians are used to compute different topological characteristics of the cell complex [20, 21]. One example are the well-known Betti numbers, which are obtained simply by [22]

$$\beta_p = \text{Dimension}(\text{Nullspace}(L_p)), \tag{3}$$

i.e., the number of zero eigenvalues of L_p. These have been used in many areas

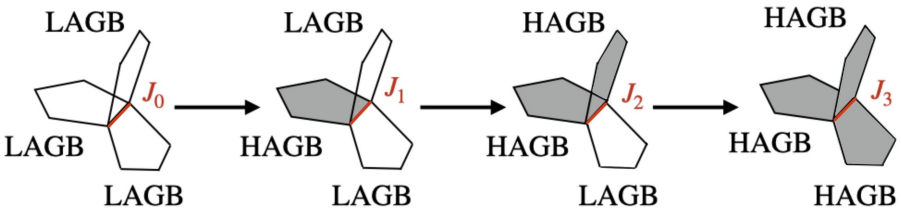

Figure 3: Illustration of triple lines/junction types. J_i is a triple line/junction with i adjacent HAGBs.

to characterise complex networks [23, 24].

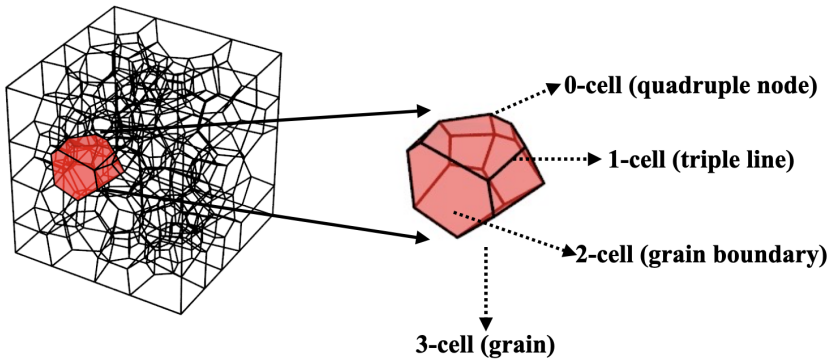

Figure 4: Cells of a 3-cell complex with different topological dimensions.

The collection of all q-cells together with the lower-dimensional cells on their boundaries is referred to as the q-skeleton of $\mathcal{M}$, denoted by $\mathcal{M}_q$: $\mathcal{M}_3$ coincides with $\mathcal{M}$; $\mathcal{M}_2$ is formed by all 2-cells, 1-cells, and 0-cells of $\mathcal{M}$; $\mathcal{M}_1$ is formed by all 1-cells and 0-cells of $\mathcal{M}$; and $\mathcal{M}_0$ is formed by all 0-cells of $\mathcal{M}$. The Laplacians of $\mathcal{M}_q$ are calculated by Eq. 2 with $\partial_{q+1} = 0$. For example $\mathcal{M}_2$ has $L_0(\mathcal{M}_2) = \partial_0 \circ \partial_0^T \equiv L_0$, $L_1(\mathcal{M}_2) = \partial_1^T \circ \partial_1 + \partial_2 \circ \partial_2^T \equiv L_1$, and $L_2(\mathcal{M}_q) = \partial_2^T \circ \partial_2 \neq L_2$, while $\mathcal{M}_1$ has $L_0(\mathcal{M}_1) = \partial_0 \circ \partial_0^T \equiv L_0$, $L_1(\mathcal{M}_q) = \partial_1^T \circ \partial_1 \neq L_1$. These Laplacians are used to calculate the Betti numbers of the skeletons by Eq. 3. The Betti numbers used in this work are: $\beta_0(\mathcal{M}_1) = \beta_0(\mathcal{M}_2)$, which gives the number of connected components of 1-cells and 2-cells; $\beta_1(\mathcal{M}_1)$ which gives the number of one-dimensional holes, i.e., closed cycles of 1-cells (2-cells are not included in $\mathcal{M}_1$); and $\beta_2(\mathcal{M}_2)$ which gives the number of two-dimensional holes, i.e. closed cycles of 2-cells (3-cells are not included in $\mathcal{M}_2$).

A sub-structure of a polycrystalline assembly with elements of dimension q is a geometric realisation of $\mathcal{M}_q$. Consider a criterion by which the elements

of the q-substructure of a given polycrystalline assembly are classified into sets with distinct characters. For example, in this work the grain boundaries are classified into two sets – LAGBs and HAGBs – and the triple lines are classified into four sets – J_0, J_1, J_2, J_3. Each set corresponds to a subset of $\mathcal{M}_q$, and the union of all sets corresponds to $\mathcal{M}_q$. Each set of elements is described by reduced boundary operators (matrices) that account for the connectivity and the relative orientations only of the elements belonging to the set. Following the general procedure for analysis of $\mathcal{M}_q$ described above, the Laplacians and Betti numbers of different q-substructures can be calculated. This is used in the work to analyse the substructures formed by the two types of grain boundaries and the four types of triple lines. For example, the set of HAGBs is a subset of $\mathcal{M}_2$, whose $\beta_2(\mathcal{M}_2)$ provides the number of grains in the polycrystalline assembly, where grain is understood as a region fully enclosed by HAGBs. Further, the set of triple lines of one type is a subset of $\mathcal{M}_1$, whose $\beta_1(\mathcal{M}_1)$ provides the number of grain boundaries fully enclosed by triple lines of this type.

Acknowledgments

Zhu acknowledges gratefully the financial support of China Scholarship Council and the University of Manchester via the joint PhD scholarship programme. Borodin and Jivkov acknowledge the financial support from EPSRC, UK via grants EP/N026136/1 and EP/V022687/1.

The authors confirm that the data supporting the findings of this study is available within the article. The raw/processed data required to reproduce these findings cannot be shared at this time due to technical or time limitations.

References

[1] V. Randle, Electron backscatter diffraction: Strategies for reliable data acquisition and processing, Materials characterization 60 (9) (2009) 913–922.

[2] V. Randle, B. Ralph, Grain boundary structure and mechanical properties, Revue de physique appliquée 23 (4) (1988) 501–512.

[3] A. Morawiec, Orientations and rotations, Springer, 2003.

[4] R. Kobayashi, J. A. Warren, Modeling the formation and dynamics of polycrystals in 3d, Physica A: Statistical Mechanics and its Applications 356 (1) (2005) 127–132.

[5] G.-h. Zhu, W.-m. Mao, Y.-n. Yu, Calculation of misorientation distribution between recrystallized grains and deformed matrix, Scripta materialia 42 (1) (1999) 37–41.

[6] O. Engler, V. Randle, Introduction to texture analysis: macrotexture, microtexture, and orientation mapping, CRC press, 2009.

[7] J. Mackenzie, Second paper on statistics associated with the random disorientation of cubes, Biometrika 45 (1-2) (1958) 229–240.

[8] O. K. Johnson, J. M. Lund, T. R. Critchfield, Spectral graph theory for characterization and homogenization of grain boundary networks, Acta Materialia 146 (2018) 42–54. doi:https://doi.org/10.1016/j.actamat.2017.11.054.
URL https://www.sciencedirect.com/science/article/pii/S1359645417310455

[9] S. Holland, X. Wang, X. Fang, Y. Guo, F. Yan, L. Li, Grain boundary network evolution in inconel 718 from selective laser melting to heat treatment, Materials Science and Engineering: A 725 (2018) 406–418.

[10] Y. Yi, J. Kim, Characterization methods of grain boundary and triple junction distributions, Scripta Materialia 50 (6) (2004) 855–859, viewpoint Set No 34. Deformation and stability of nanoscale metallic multilayers. doi:https://doi.org/10.1016/j.scriptamat.2003.12.010.

[11] M. Frary, C. A. Schuh*, Connectivity and percolation behaviour of grain boundary networks in three dimensions, Philosophical Magazine 85 (11) (2005) 1123–1143.

[12] E. Borodin, A. Jivkov, Evolution of triple junctions' network during severe plastic deformation of copper alloys–a discrete stochastic modelling, Philosophical Magazine 100 (4) (2020) 467–485.

[13] S. Zhu, E. Borodin, A. P. Jivkov, Triple junctions network as the key pattern for characterisation of grain structure evolution in metals, Materials & Design 198 (2021) 109352.

[14] J. May, A Concise Course in Algebraic Topology, University of Chicago Press, 1999.

[15] V. V. Dremov, P. V. Chirkov, A. V. Karavaev, Molecular dynamics study of the effect of extended ingrain defects on grain growth kinetics in nanocrystalline copper, Scientific Reports 11 (2021) 934.

[16] R. Perumal, P. K. Amos, M. Selzer, B. Nestler, Phase-field study of the transient phenomena induced by abnormally large grains during 2-dimensional isotropic grain growth, Computational Materials Science 147 (2018) 227–237.

[17] D. Zöllner, P. Streitenberger, Three-dimensional normal grain growth: Monte carlo potts model simulation and analytical mean field theory, Scripta materialia 54 (9) (2006) 1697–1702.

[18] K. Janssens, An introductory review of cellular automata modeling of moving grain boundaries in polycrystalline materials, Mathematics and Computers in Simulation 80 (7) (2010) 1361–1381.

[19] G. E. Cooke, R. L. Finney, Homology of Cell Complexes, Princeton University Press, 1967.

[20] P. v. Mieghem, Graph Spectra for Complex Networks, Cambridge University Press, 2010. doi:10.1017/CBO9780511921681.

[21] M. Weber, E. Saucan, J. Jost, Characterizing complex networks with forman-ricci curvature and associated geometric flows, Journal of Complex Networks 5 (4) (2017) 527–550. doi:10.1093/comnet/cnw030.

[22] J. Friedman, Computing betti numbers via combinatorial laplacians, Algorithmica 21 (4) (1998) 331–346.

[23] M. E. Aktas, E. Akbas, A. El Fatmaoui, Persistence homology of networks: methods and applications, Applied Network Science 4 (1) (2019) 1–28.

[24] S. Agami, R. J. Adler, Modeling of persistent homology, Communications in Statistics-Theory and Methods 49 (20) (2020) 4871–4888.